THE JOURNAL OF PHYSICAL CHEMISTRY B

Article

pubs.acs.org/JPCB

Quantum Mechanics/Molecular Mechanics Study of Oxygen Binding in Hemocyanin

Toru Saito and Walter Thiel*

Max-Planck-Institut für Kohlenforschung, Kaiser-Wilhelm-Platz 1, D-45470 Mülheim an der Ruhr, Germany

Supporting Information

ABSTRACT: We report a combined quantum mechanics/molecular mechanics (QM/MM) study on the mechanism of reversible dioxygen binding in the active site of hemocyanin (Hc). The QM region is treated by broken-symmetry density functional theory (DFT) with spin projection corrections. The X-ray structures of deoxygenated (deoxyHc) and oxygenated (oxyHc) hemocyanin are well reproduced by QM/MM geometry optimizations. The computed relative energies strongly depend on the chosen density functional. They are consistent with the available thermodynamic data for oxygen binding in hemocyanin and in synthetic model complexes when the BH&HLYP hybrid functional with 50% Hartree−Fock exchange is used. According to the QM(BH&HLYP)/MM results, the reaction proceeds stepwise with two sequential electron transfer (ET) processes in the triplet state followed by an intersystem crossing to the singlet product. The first ET step leads to a nonbridged superoxo $Cu_B^{II}-O_2^{\bullet-}$ intermediate via a low-barrier transition state. The second ET step is even more facile and yields a side-on oxyHc complex with the characteristic Cu_2O_2 butterfly core, accompanied by triplet-singlet intersystem crossing. The computed barriers are very small so that the two ET processes are expected to very rapid and nearly simultaneous.

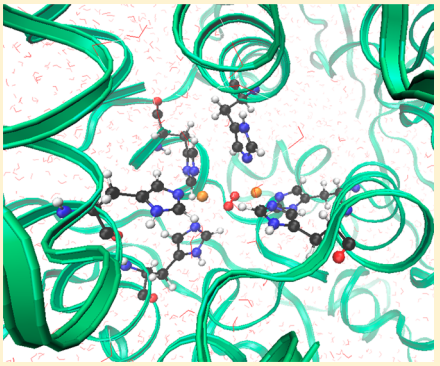

1. INTRODUCTION

Hemocyanin (Hc) is an oxygen transport protein that binds and releases molecular oxygen reversibly; it is found in mollusks and arthropods.[1−7] The active site of Hc contains two copper atoms, each of which is coordinated by three histidines. The oxygen binding process can be described by a two-state model as in the case of hemoglobin.[8] Many structural, kinetic, and spectroscopic studies have addressed the spin-forbidden reaction of reversible O_2 binding.[9−17] The use of synthetic models has allowed important insights into the possible O_2 coordination modes in the active site.[9−14] According to X-ray crystallographic analyses, both the deoxygenated (deoxy) and oxygenated (oxy) forms of subunit II in *Limulus polyphemus* adopt the low oxygen affinity T-state, where the separations between the two copper ions are 4.6 ± 0.2 Å for deoxyHc and 3.6 ± 0.2 Å for oxyHc (Scheme 1).[5,6] The binding of the triplet oxygen molecule between the two Cu^I ions in deoxyHc requires two electron transfers (ET) and one intersystem crossing (ISC).

This oxygenation process shortens the $Cu_A\cdots Cu_B$ distance by ca. 1.0 Å, while the remaining geometric parameters (including those of the metal-ligating histidine residues) do not change significantly. Parallel stacking and hydrogen bonding between the metal-ligating histidines and the surrounding residues (e.g., $\pi-\pi$ stacking interaction between His328 and Phe49) are considered to be important for the structural similarity between oxyHc and deoxyHc.[5] The binuclear copper center of oxyHc (μ-η^2:η^2 peroxide Cu_2O_2 core) is known to be diamagnetic, exhibiting a strong antiferromagnetic interaction ($2J < -600$ cm^{-1}).[17] The μ-η^2:η^2 peroxide Cu_2O_2 core is also found in tyrosinase, which has an active site similar to Hc and catalyzes the oxidation of phenol to *o*-quinone.[18] Because it is well-known that metal−oxo species play an important role in hydroxylation reactions, the electronic structure of μ-η^2:η^2 peroxo dicopper(II) complexes and other relevant species such as bis(μ-oxo) dicopper(III) complexes has attracted considerable attention from both the theoretical and experimental side.[19−28]

Scheme 1. Illustration of deoxyHc (PDB Code: 1LLA) and oxyHc (PDB Code: 1OXY) from *Limulus polyphemus*[a]

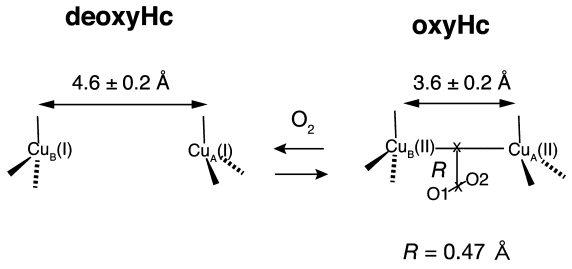

[a]The distance between the center of mass of O1−O2 and of Cu_A-Cu_B is denoted as *R*.

Received: January 13, 2014
Revised: April 23, 2014
Published: April 24, 2014

   dx.doi.org/10.1021/jp5003885 | *J. Phys. Chem. B* 2014, 118, 5034−5043

Scheme 2. Mechanism of O_2 Binding from deoxyHc + O_2 (1) to oxyHc (3) via a Nonbridged Superoxo Complex (2a) or an End-on η^1-η^1 Peroxo-like Species (2b)

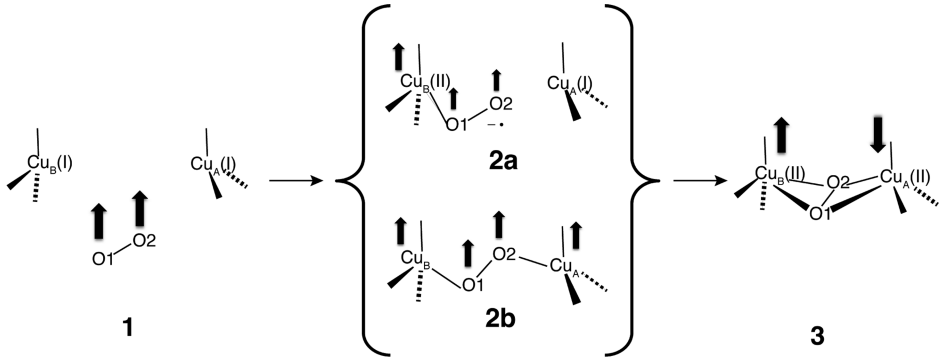

Concerning the oxygenation mechanism, early spectroscopic and kinetic studies on model compounds suggested that a mononuclear superoxide adduct has been observed to precede the formation of a μ-η^2:η^2 peroxide species.[9,12] In the biomimetic dicopper complex with a bridging *N,N,N′,N′*-bis{2-(2-pyridyl)ethyl}-1,4-butanediamine ligand (N4), the end-on η^1-η^1 peroxo (**2b**) and the side-on μ-η^2:η^2 peroxo (**3**) species were both observed, with the latter being thermodynamically favored (ΔH) by 7.2 kcal mol^{-1}, whereas a nonbridged superoxo $Cu_B^{II}-O_2^{\bullet-}$ species (**2a** in Scheme 2) was not detected;[12] the activation enthalpies for formation of **2a** and **3** were reported as 0 and 4.3 kcal mol^{-1}, respectively.[12] Hirota et al. examined the activation enthalpy and entropy of oxygen binding in Hc proteins using flash photolysis and complementary K-edge X-ray absorption spectroscopy.[15] The measured activation enthalpy for *Carcinus aestuarii* Hc (7.2 kcal mol^{-1}) was similar to that of a model complex (4.3 kcal mol^{-1}, see above).[12] The small activation barriers can be taken as support for a nearly simultaneous ET process.[15,16]

Several quantum mechanics (QM) studies have addressed the O_2 binding/release mechanism of Hc.[29−35] They employed model complexes and involved partial geometry optimizations along a reaction coordinate *R*, the distance between the center of mass of O1−O2 and of $Cu_A\cdots Cu_B$ (Scheme 1). Solomon and co-workers investigated the O_2 binding process at the UB3LYP/LANL2DZ level using a small model with ammonia ligands.[30] On the basis of the changes in the electronic structure of several partially optimized structures along *R*, they concluded that a simultaneous two-electron transfer occurs to give an end-on η^1-η^1 peroxo-like complex (**2b** in Scheme 2), followed by triplet-to-singlet ISC in the μ-η^1:η^2 coordination mode around R = 0.6 Å. Their optimized oxy form with μ-η^2:η^2 coordination had a planar Cu_2O_2 core with R = 0.0 Å, whereas the crystal structure of oxyHc contains a bent butterfly moiety (R = 0.47 Å, Scheme 1). In a more recent study, they revisited the reaction at the UB3LYP/TZVP level using a larger model with methylimidazole ligands. The potential energy surface scans along the $Cu_A\cdots Cu_B$ distance with frozen methyl carbon atoms also supported a simultaneous ET mechanism.[35] The ISC point was estimated to occur in the μ-η^1:η^2 coordination mode with a $Cu_A\cdots Cu_B$ distance of ca. 3.9 Å, leading to a bent μ-η^2:η^2 peroxo structure (**3**). These computational studies provided valuable information about the spin-forbidden O_2 binding to Hc, suggesting that it proceeds via an exothermic simultaneous ET process.

The QM-only approach to O_2 binding to Hc is faced with the problem of choosing a realistic model system. Indeed, at the QM-only level, model complexes of deoxyHc end up dissociating into two $[Cu^IL_3]^+$ (L = NH_3, imidazole, methylimidazole) fragments when full unconstrained geometry optimizations are performed.[30,35] Also, QM-only models without the protein environment do not yield an intermediate or transition state (TS) unless some atoms or structural parameters are kept fixed. This makes it difficult to investigate the overall O_2 binding/release reaction. In terms of electronic structure, theoretical modeling of the Cu_2O_2 core is challenging due to its multireference character. Spin unrestricted (broken-symmetry) density functional theory (UDFT) as well as coupled cluster and multireference wave function methods have been benchmarked so far,[21−29] but there are still many problems to overcome. UDFT results heavily depend on the chosen functional and often do not show systematic behavior.[21−24] Multireference wave function methods starting from closed-shell molecular orbitals require a large active space because the reference wave function is likely to suffer from triplet instability. Also, the complicated interplay between nondynamical and dynamical electron correlation effects[25] must be treated in a balanced manner at different geometrical arrangements. In addition, relativistic effects make important contributions to the relative energies.[27]

In this article, we examine whether the O_2 binding proceeds through simultaneous or sequential ET steps. We determine the relevant TS and intermediate structures using the mixed quantum mechanics/molecular mechanics (QM/MM) method, which has emerged as a robust and realistic approach for investigating enzymatic reactions.[36−39] We select a QM/MM model for the solvated enzyme that enables us to perform geometry optimizations with full relaxation of the active-site region. Because multireference wave function calculations are not yet feasible for systems of this size, we apply several pure and hybrid UDFT methods as QM components. To the best of our knowledge, this is the first study of the reversible O_2 binding in Hc at the QM/MM level.

2. METHODS

2.1. System Setup. The initial coordinates were taken from the X-ray structure of oxyHc from *Limulus polyphemus* (PDB code: 1OXY, resolution 2.4 Å).[5] The 55 missing residues (18−32, 132−150, 421−427, 522−530, 570−573, and 628) were added by using MODELER (ver. 9.11).[40] All these residues are more than 20 Å away from the two copper atoms (Figure S1 in Supporting Information). The protonation states of titratable residues (His, Glu, Asp) were assigned on the basis of pK_a values obtained from the PROPKA program,[41] in combination

dx.doi.org/10.1021/jp5003885 | J. Phys. Chem. B 2014, 118, 5034−5043

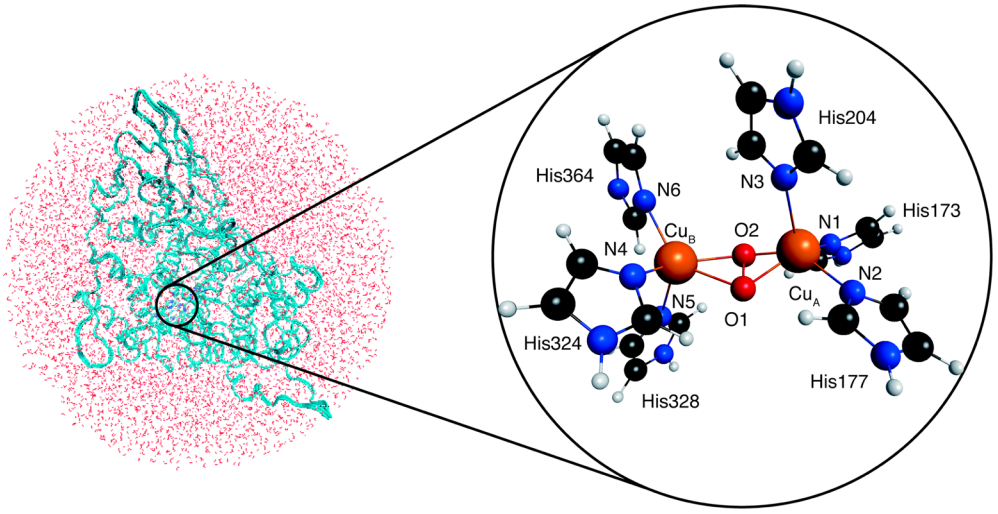

Figure 1. QM/MM Model (Left) and QM Subsystem (Right) Defined in This Study

with visual inspection. The missing atomic charges on the Cu_2O_2 core were determined by fitting the electrostatic potential by the CHELPG method,[42] with the radius for Cu set to 2.0 Å.[43] The Lennard-Jones parameters described by Ungar et al.[44] were used for copper. Hydrogen atoms were added by the HBUILD module as implemented in CHARMM.[45] The sulfur atoms involved in the two disulfide bonds (Cys534-Cys576 and Cys536-Cys583) were not protonated.

The initial classical molecular dynamics (MD) simulations were performed with the CHARMM program in a similar way as in previous studies from our group.[46−48] The enzyme was solvated in a water ball of 45 Å radius centered at the center of mass.[49] Two distant crystal water molecules (891 and 947), which are more than 45 Å away from the center, were deleted. The total charge of the initially built system was −7e. To neutralize this charge, solvent water molecules that were at least 5.5 Å away from any protein atoms were replaced by Na^+ and Cl^- ions. Then, a 500 ps MD equilibration run at 300 K with a time step of 1 fs was conducted followed by energy minimization and heating. Residues further away than 20 Å from the Cu_2O_2 core (including the added residues noted above) were kept fixed during the MD simulations. The Cu_2O_2 core and the metal-ligating histidine residues were also kept frozen. The equilibrated system contained 40 050 atoms in total, including 9697 TIP3P water molecules, as shown in Figure 1. The Supporting Information provides further details on the setup procedure.

2.2. QM/MM Computations. We used the final snapshot from the MD trajectory as the initial geometry for the QM/MM optimization of oxyHc. As can be seen from Figure 1, the QM subsystem of oxyHc consists of the Cu_2O_2 core and the imidazole groups of the six ligating histidine residues (His173, His177, His204, His324, His328, and His364). As mentioned above, the electronic structure in the Cu_2O_2 core, and especially the degree of singlet diradical character, is sensitive to the amount of Hartree−Fock (HF) exchange in DFT hybrid functionals. Thus, we used functionals with different amounts of HF exchange, namely BLYP (0%), B3LYP (20%), BH&HLYP (50%), and M06-2X (54%).[50−54] We also employed the range-separated CAM-B3LYP functional, which contains fractions of HF exchange ranging from 19% to 65%.[55] The TZVP basis set was used to describe the QM region (52 QM atoms and 6 hydrogen link atoms for oxyHc; 818 spherical basis functions).[56] The broken-symmetry approach was applied in the QM calculations. Unless otherwise noted, we performed open-shell singlet calculations and corrected the energies of the singlet states (E^S) using an approximate spin projection method:[57,58]

$$E^S = \frac{\langle \hat{\mathbf{S}}^2 \rangle^T E^{BS} - \langle \hat{\mathbf{S}}^2 \rangle^{BS} E^T}{\langle \hat{\mathbf{S}}^2 \rangle^T - \langle \hat{\mathbf{S}}^2 \rangle^{BS}} \quad (1)$$

where BS and T represent the broken-symmetry (open-shell) singlet and triplet state, respectively. E^X and $\langle \hat{\mathbf{S}}^2 \rangle^X$ denote the total energy and the expectation value of total spin angular momentum for spin state X (X = BS, T), respectively. The QM/MM computations were carried out using a development version of the ChemShell package (ver. 3.5).[59,60] We employed the electronic embedding scheme, in which the electrostatic interactions of the QM electrons with the fixed MM point charges (q_{MM}) are included in the one-electron integrals. No cutoff was introduced for the electrostatic interactions. The link atom method with the charge shift model was used at the boundary between the QM and MM regions. The QM subsystem was treated by the Gaussian09 program package,[61] whereas the MM subsystem was described by the CHARMM22 force field as implemented in the DL_POLY program.[62]

Within ChemShell, the conventional Gaussian interface uses the *Massage* keyword to compute the forces on the MM point charges ($\mathbf{F}_{MM}$) arising from the interaction with the QM atoms. It should be noted that this keyword regards the MM atoms as ghost atoms, implying the need to allocate extra memory for their basis functions and the grid points for numerical integration. When dealing with a system consisting of several tens of thousands of MM atoms, hundreds of GB RAM are allocated during the calculation. This is obviously impractical and unnecessary. Therefore, we have modified the Gaussian interface of the ChemShell program such that by default $\mathbf{F}_{MM}$ is calculated more efficiently from the electric field ($\mathbf{E}$) at the MM atoms as

$$\mathbf{F}_{MM} = q_{MM}\mathbf{E} \quad (2)$$

The *Charge*, *Density*, and *Prop = (Read, Field)* keywords are applied to calculate $\mathbf{E}$ in analogy with an AMBER-Gaussian interface.[63] Unlike the conventional method, the new

dx.doi.org/10.1021/jp5003885 | J. Phys. Chem. B 2014, 118, 5034−5043

Table 1. X-ray and QM/MM Optimized Distances in deoxyHc (Å)

parameters[a]	X-ray[b]	RBLYP	RB3LYP	RBH&HLYP	RM06-2X	RCAM-B3LYP
$Cu_A\cdots Cu_B$	4.61	4.55	4.54	4.51	4.25	4.55
Cu_A–N1	2.01	2.03	2.04	2.06	2.08	2.03
Cu_A–N2	2.01	2.07	2.07	2.09	2.11	2.06
Cu_A–N3	1.94	1.99	2.00	2.02	2.05	1.99
Cu_B–N4	2.17	2.00	2.01	2.03	2.05	2.00
Cu_B–N5	2.08	2.01	2.02	2.04	2.08	2.01
Cu_B–N6	1.92	1.97	1.98	1.99	2.03	1.97

[a]See Figure 1. [b]From ref 6.

Table 2. X-ray and QM/MM Optimized Structural Parameters[a] and 2J Values[b] in Singlet oxyHc

geometry	$Cu_A\cdots Cu_B$	O1–O2	Cu_A–O1–Cu_B	Cu_A–O2–Cu_B	eq Cu–N[e]	ax Cu–N[e]	R	2J
UBLYP	3.71	1.43	127.4	129.2	2.03	2.20	0.54	−1974
UB3LYP	3.54	1.42	121.6	122.0	2.02	2.22	0.68	−983
UBH&HLYP	3.45	1.47	122.7	122.9	2.03	2.23	0.59	−1303
UM06-2X	3.39	1.48	117.8	117.7	2.03	2.23	0.71	−895
UCAM-B3LYP	3.47	1.42	121.4	121.6	2.01	2.21	0.66	−1171
oxyHc (X-ray)[c]	3.59	1.41	120.8	143.1	2.21	2.42	0.47	<−600
oxyTy (X-ray)[d]	3.55	1.50	120.9	123.3	2.13	2.18	0.63	<−600

[a]In Å for distances and in degree for angles. [b]In cm^{-1}. [c]From ref 5, oxyHemocyanin, resolution of 2.4 Å. [d]From ref 18, oxyTyrosinase, resolution of 1.5 Å. [e]Average values, eq (equatorial) and ax (axial).

procedure requires a negligibly small amount of CPU time and RAM.

Geometry optimizations of the active-site region (990 atoms for oxyHc, Supporting Information) were performed in hybrid delocalized internal coordinates (HDLC)[64] for both the singlet and triplet states using DL-FIND,[65] which is part of the ChemShell program. During the optimizations, the positions of all MM atoms more than 10 Å away from either of the copper ions were kept frozen. The quasi-Newton limited-memory Broyden–Fletcher–Goldfarb–Shannon (L-BFGS) method was used to search for minima.[66] TS structures were optimized by the dimer method,[67,68] with the weights being set to 1 for all QM atoms and to 0 for all MM atoms. Minimum energy crossing points (MECPs) between singlet and triplet surfaces were located using the algorithm proposed by Harvey.[69−71] This method requires the energies and gradients for BS and T states that are used to generate an effective gradient,

$$\mathbf{g}^{\mathrm{eff}} = \Delta E \Delta \mathbf{g} + \alpha \left(\mathbf{g}^{\mathrm{BS}} - \frac{\Delta \mathbf{g}}{|\Delta \mathbf{g}|} \mathbf{g}^{\mathrm{BS}} \frac{\Delta \mathbf{g}}{|\Delta \mathbf{g}|} \right) \tag{3}$$

where

$$\Delta E = E^{\mathrm{BS}} - E^{\mathrm{T}} \tag{4}$$

$$\Delta \mathbf{g} = \mathbf{g}^{\mathrm{BS}} - \mathbf{g}^{\mathrm{T}} \tag{5}$$

and α is a parameter.[70] According to eq 2, the spin projected energy E^{S} is equivalent to E^{T} at the MECP. The QM/MM MECP optimizations were carried out with a modified version of the Gaussian interface in ChemShell. The convergence criteria on ΔE and on the root-mean-square (RMS) gradient were set to 0.05 mE_h and 0.001 E_h $Bohr^{-1}$, respectively.[69]

3. RESULTS AND DISCUSSION

In this section, we present the QM/MM optimized structures of all relevant points, the computed QM/MM energy profiles for O_2 binding, and an analysis of the influence of the protein environment. The Cartesian coordinates of all optimized stationary points are listed in the Supporting Information.

3.1. Optimized Structures of deoxyHc and oxyHc.

We first address the computed geometries of deoxyHc and oxyHc to assess the reliability of our QM/MM approach. We first note that the new Gaussian QM/MM interface in ChemShell provides results that are essentially identical to those obtained with the standard TURBOMOLE[72] interface. For oxyHc and QM=BH&HLYP/TZVP, the RMS deviation in the optimized structures is only 0.003 Å, and the total QM/MM energies differ by only 0.04 mE_h, when either Gaussian09 or TURBOMOLE was used as the QM code in the QM/MM geometry optimization (see Supporting Information for details). The starting geometry for deoxyHc was generated from the initially constructed geometry of oxyHc (section 2.2) simply by deleting the O_2 moiety. The Cu ions were always assigned a formal charge of +1. The QM/MM geometry optimizations were performed using spin-restricted DFT calculations for the QM region because deoxyHc has a closed-shell configuration.

Starting from an oxyHc-type initial structure with a $Cu_A\cdots Cu_B$ distance of ca. 3.6 Å (see above), the QM/MM geometry optimizations for deoxyHc lead to a substantial elongation of the $Cu_A\cdots Cu_B$ distance (typically by almost 1 Å). Except for QM=RM06-2X, the optimized $Cu_A\cdots Cu_B$ distances are in the range of 4.51–4.55 Å for all functionals, in excellent agreement with the X-ray value (Table 1). The $Cu_A\cdots Cu_B$ separation tends to be significantly shorter when functionals that take into account dispersion are used. For example, QM/MM geometry optimization with QM=RB3LYP-D3[73] yields a $Cu_A\cdots Cu_B$ distance of 4.25 Å (as with QM=RM06-2X).

Next, we focus on the optimized structures of singlet oxyHc (^{1}**3**). Table 2 shows that the computed values of the diabatic singlet–triplet energy splitting, $2J = E^{\mathrm{S}}(^1\mathbf{3}) - E^{\mathrm{T}}(^1\mathbf{3})$, are compatible with the observed diamagnetism ($2J < -600$ cm^{-1}). The optimized $Cu_A\cdots Cu_B$ distances vary depending on the chosen functional. They cover a fairly wide range (3.39–3.71 Å) that includes the experimental value (best reproduced with QM=UB3LYP, Table 2). The Cu_A–O1–Cu_B and Cu_A–O2–Cu_B angles are quite similar to each other in each of the

dx.doi.org/10.1021/jp5003885 | J. Phys. Chem. B 2014, 118, 5034−5043

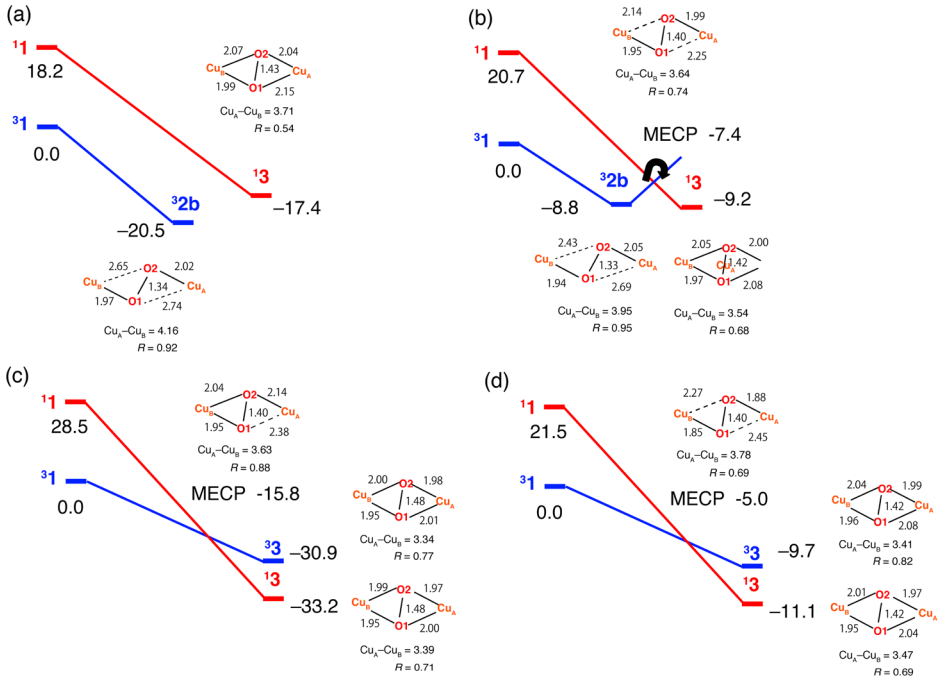

Figure 2. Comparison between the QM/MM results for the singlet (in red) and triplet (in blue) minima using (a) UBLYP, (b) UB3LYP, (c) UM06-2X, and (d) UCAM-B3LYP for the QM region. Bond lengths and energies are given in Å and kcal mol^{-1}, respectively.

optimized QM/MM structures (regardless of the chosen functional), consistent with QM-only studies of truncated model complexes,[33] which indicates that the inclusion of the surrounding protein does not affect the shape of the Cu_2O_2 core. These two angles are also close to each other in the high-resolution X-ray structure of oxyTy but differ by more than 20° in the low-resolution X-ray structure of oxyHc (Table 2). The average equatorial Cu−N bond lengths (2.01−2.03 Å) are computed to be significantly shorter than the axial Cu−N bond lengths (2.20−2.23 Å), in qualitative agreement with the trend in the X-ray structure (Table 2). More quantitative comparisons are hampered by the low accuracy of the X-ray structure of oxyHc (resolution: 2.4 Å). It has previously been suggested that DFT-based optimized distances (e.g., for metal−oxo bonds) may be closer to high-resolution than to low-resolution X-ray data.[74] We note that the QM/MM optimized geometries of oxyHc are indeed generally rather similar to the X-ray structure of oxyTyrosinase (resolution: 1.5 Å),[18] which also contains the butterfly Cu_2O_2 moiety (Table 2).

3.2. QM/MM Energy Profiles for O_2 Binding. The sum of the total QM/MM energy of deoxyHc and of the QM energy of the isolated $^{1,3}O_2$ molecule defines the reference energies for the singlet and triplet states (^{1,3}**1**). The energy difference between ^{1}**1** and ^{3}**1** is the adiabatic singlet−triplet energy gap of O_2. The calculated values of 18.2, 20.7, 24.3, and 21.5 kcal mol^{-1} for UBLYP, UB3LYP, UBH&HLYP, and UCAM-B3LYP are in good agreement with the experimental value of 22.5 kcal mol^{-1},[75] which is, however, overestimated by UM06-2X (28.5 kcal mol^{-1}). Let us recall that UDFT and UDFT/MM calculations with spin projection can describe reactions involving diradical-like species realistically at low computational cost.[76−78] We consider both the singlet and triplet energy surfaces to compare the reactions of the two spin states, although it is well-known that the early stage of oxygenation proceeds on the triplet surface. We will therefore discuss the potential energies relative to ^{3}**1**.

Figure 2 illustrates barrier-free oxygen binding in QM/MM geometry optimizations obtained with functionals other than BH&HLYP (for BH&HLYP, see below and Figure 3). For these functionals, all attempts failed to locate stationary points between **1** and **3** (e.g., a substrate complex or transition state). These results are inconsistent with the experimentally observed small barrier in Hc.[15] For the triplet minimum, BLYP and B3LYP tend to give an end-on η^1-η^1 coordination (^{3}**2b**), whereas CAM-B3LYP and M06-2X yield a side-on μ:η^2-η^2 species (^{3}**3**). The UBLYP method overstabilizes the end-on η^1-η^1 intermediate ^{3}**2b**, lying 3.1 kcal mol^{-1} below the singlet oxyHc form (^{1}**3**). Because the triplet minimum ^{3}**2b** has not yet been detected as a stable species experimentally, pure DFT functionals such as BLYP are not capable of predicting the correct singlet ground state, as has already been demonstrated by previous QM-only studies.[30,32] Upon inclusion of HF exchange the singlet oxyHc form ^{1}**3** becomes most stable. The QM(B3LYP)/MM calculations predict a stepwise mechanism, i.e., the formation of an end-on η^1-η^1 superoxo-like intermediate (^{3}**2b**) followed by an ISC step to give the oxyHc form (^{1}**3**). The MECP contains a bridging O_2 moiety (between μ:η^1-η^2 and μ:η^1-η^1) with a $Cu_A\cdots Cu_B$ distance of 3.64 Å and R of 0.74 Å, which lies 1.4 kcal mol^{-1} above the triplet minimum ^{3}**2b**. On the other hand, M06-2X and CAM-B3LYP support a single-step mechanism, without changes in bond connectivity during the ISC step. The experimental reaction enthalpy[79] of −11.5 to −6.0 kcal mol^{-1} is reproduced reasonably well by the QM/MM reaction energy for QM=UB3LYP (−9.2 kcal mol^{-1}) and QM=UCAM-B3LYP (−11.1 kcal mol^{-1}) but is significantly overestimated for QM=M06-2X (−33.2 kcal mol^{-1}).

The results from the QM(UBH&HLYP)/MM calculations are different and compatible with the available experimental data. The mechanism is found to be stepwise with two sequential ET processes. The first ET step via ^{3}**TS1** leads to the formation of the Cu_B−O1 bond and a superoxo Cu_B^{II}−$O_2^{\bullet-}$ intermediate (^{3}**2a**), the second ET step via ^{3}**TS2** generates the

dx.doi.org/10.1021/jp5003885 | J. Phys. Chem. B 2014, 118, 5034−5043

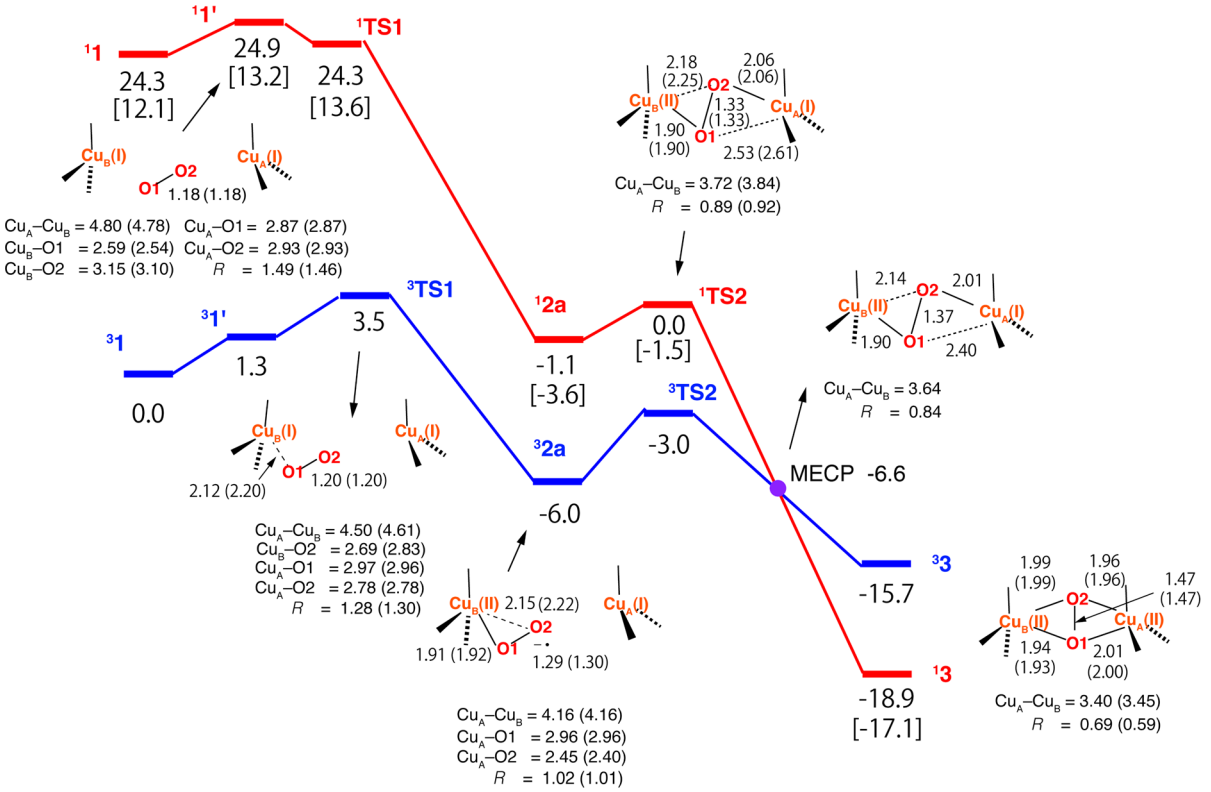

Figure 3. QM(UBH&HLYP/TZVP)/MM potential energy profile for the singlet (E^S [E^{BS}] in red) and the triplet (E^T in blue) and selected optimized distances for the triplet and the singlet (in parentheses). Bond lengths and energies are given in Å and kcal mol^{-1}, respectively.

Cu_A–O1 bond, and the subsequent ISC from the triplet to the singlet yields oxyHc (^{1}**3**), as shown in Figure 3. The QM(UBH&HLYP)/MM geometry optimizations for the triplet and singlet states give minima corresponding to a substrate complex (deoxyHc + $^{1,3}O_2$) (^{1,3}**1**′). The interaction between the two Cu ions and O_2 is negligibly small in ^{1,3}**1**′ judging from the large Cu–O separations. The spin densities on Cu_A, Cu_B, O1, and O2 in ^{3}**1**′ are 0.00, 0.02, 0.99, and 0.99, respectively. The presence of a superoxo intermediate is consistent with observations in synthetic model complexes. We note that geometry optimizations using the other functionals did not succeed in locating minima corresponding to ^{1,3}**1**′, even when starting from BH&HLYP-optimized geometries. We also tested other initial structures, with O_2 being moved from the BH&HLYP-optimized position to a reaction coordinate value of R = 3.0 Å, where the interaction between two Cu ions and the O_2 molecule should be negligible; however, the subsequent geometry optimizations yielded other minima: ^{1}**3** and ^{3}**2b** for BLYP and B3LYP and ^{1,3}**3** for CAM-B3LYP and M06-2X.

Returning to the QM(BH&HLYP)/MM results, the highest activation barrier on the computed pathway (^{3}**TS1**) is ca. 4 kcal mol^{-1} lower than the experimental activation enthalpy (3.5 versus 7.2 kcal mol^{-1}). The singlet transition state ^{1}**TS1** is 0.4 kcal mol^{-1} higher in energy than ^{1}**1**′ in the uncorrected broken-symmetry calculation (E^{BS}) but lies 0.6 kcal mol^{-1} lower than ^{1}**1**′ after applying the energy correction (E^S). The one-electron transfer via ^{3}**TS1** leads to the triplet intermediate ^{3}**2a** that is 6.0 kcal mol^{-1} more stable than ^{3}**1**. The singlet intermediate ^{1}**2a** is also 1.1 kcal mol^{-1} below ^{3}**1**. The spin densities on Cu_A, Cu_B, O1, and O2 in ^{3}**2a** (^{1}**2a**) are 0.01 (−0.01), 0.65 (0.75), 0.62 (−0.33), and 0.62 (−0.51), respectively, indicating that the formal charge of the Cu_A ion in **2a** is still +1. The Cu_A–Cu_B separation in ^{3}**2a** (^{1}**2a**) is significantly shortened by 0.35 (0.45) Å compared with that in ^{3}**TS1** (^{1}**TS1**), whereas the Cu_A–O distances still remain much longer than the Cu_B-O distances.

All attempts to locate an end-on η^1-η^1 structure (**2b**) failed, which implies that UBH&HLYP favors two sequential ET processes over a simultaneous ET mechanism. Judging from the two Cu_B–O distances of 1.91 and 2.15 Å, the coordination mode of the nonbridged superoxo intermediate (^{3}**2a**) is between end-on (η^1) and side-on (η^2). For comparison, the two Cu_B-O distances in the η^1 model complex with the 1,1,1-tris[2-[N^2-(1,1,3,3-tetramethylguanidino)ethyl]amine (TMG3tren) ligand[80] are very different (1.93 vs 2.84 Å), whereas they are identical in the η^2 model complex with the hydrotris(3-*tert*-butyl-5-isopropyl-1-pyrazolyl)borate (HB(3-^{t}Bu-5-^{i}Prpz)$_3$) ligand[11] (1.84 Å). The optimized Cu_B–O1–O2 angle of ^{3}**2a** (81.2°) is closer to that of the η^2 model complex (70.6°) than that of the η^1 model complex (123.5°), whereas the optimized O1–O2 distance of ^{3}**2a** (1.29 Å) better matches the η^1 value (1.28 Å) than the η^2 value (1.22 Å). In view of this situation, it is not possible to clearly assign ^{3}**2a** as an η^1 and η^2 species, and we will thus use the neutral term "nonbridged".

Concerning the electronic structure of ^{3}**2a**, the two magnetic orbitals correspond to the superoxide π_v^* orbital and the Cu d_{xy} orbital, with the latter showing some antibonding interaction with the superoxide π_σ^* orbital (Figure S2 in Supporting Information),[4] which actually resembles the interactions in the singlet ground state of the bridged η^2 model complex[81] rather than the d_{z^2}–π_σ^* interaction found in the η^1 model complex with a triplet ground state.[4,82] On the other hand, the nonbridged species **2a** has a triplet ground state (Figure 3), in accordance with spectroscopic observations and DFT

dx.doi.org/10.1021/jp5003885 | J. Phys. Chem. B 2014, 118, 5034−5043

Table 3. Calculated Energies Relative to ^{3}1 (kcal mol^{-1})

model	^{3}1 (^{1}1)	^{3}1′ (^{1}1′)	^{3}TS1 (^{1}TS1)	^{3}2a (^{1}2a)	^{3}TS2 (^{1}TS2)	^{3}3 (^{1}3)
QM(gas)	0.0 (24.3)	1.7 (25.6)	6.1 (26.6)	−1.0 (4.2)	3.0 (6.2)	−10.5 (−13.9)
QM(pc)	0.0 (24.3)	2.4 (26.2)	6.5 (26.9)	−0.8 (4.1)	2.9 (5.9)	−9.8 (−12.8)
QM(PCM)	0.0 (24.3)	2.5 (26.0)	6.8 (27.0)	−1.6 (2.8)	2.1 (5.3)	−10.7 (−14.3)
QM/MM	0.0 (24.3)	1.3 (24.9)	3.5 (24.3)	−6.0 (−1.1)	−3.0 (0.0)	−15.7 (−18.9)

calculations on other η^1 species.[82] In previous computational work on the η^2 complex with the HB(3-^{t}Bu-5-^{i}Prpz)$_3$ ligand,[81] only pure UDFT calculations (UBP86) gave the experimentally observed singlet ground state whereas hybrid UDFT calculations with B3LYP (20% HF exchange) and UB38HFP86 (38% HF exchange) incorrectly predicted a triplet ground state. In contrast, in the present case, the chosen pure DFT functional (BLYP) is not capable of predicting the overall reaction mechanism of Hc (Figure 2). This again underscores the strong sensitivity of the UDFT results for systems containing the Cu_2O_2 core: the suitability of a given DFT functional may apparently vary with changes in the ligand environment of the copper−oxo part.

According to the QM(BH&HLYP)/MM results, the coordination mode changes during the course of the reaction from the intermediate situation in ^{3}**2a** to μ:η^1-η^1, and then the Cu_A−O1 adduct forms via ^{1,3}**TS2** to yield a bridging side-on μ:η^2-η^2 peroxo complex (^{1,3}**3**). The $Cu_A\cdots Cu_B$ distance further decreases by 0.32 (0.39) Å in ^{3}**3** (^{1}**3**) compared with that in ^{3}**TS2** (^{1}**TS2**). In the optimized ^{3}**TS2** (^{1}**TS2**), the spin densities on Cu_A increase to 0.16 (−0.21), indicating a partial ET from Cu_A to the bridging superoxo moiety. The triplet transition state (^{3}**TS2**) lies 3.0 kcal mol^{-1} above ^{3}**2a**, and its singlet counterpart (^{1}**TS2**) is 3.1 kcal mol^{-1} above ^{3}**TS2** (Figure 3). Because the singlet oxyHc form (^{1}**3**) is 3.2 kcal mol^{-1} below the triplet (^{3}**3**), the ISC from triplet to singlet must occur after **TS2**. The spin crossover is expected to be rapid because the reaction is exothermic and takes place without any change in atom connectivity.[71] The MECP is calculated to be 12.3 kcal mol^{-1} above ^{1}**3** and has a μ-η^1:η^2 coordination mode. The total energies for the MECP are given in the Supporting Information.

Overall, the rate-determining step is found to be the initial Cu_B−O1 bond formation step in accordance with studies on synthetic model complexes[12] and Hc.[15] The computed barrier heights for ^{3}**TS1** and ^{3}**TS2** are rather small; i.e., the O_2 binding process should be very fast. Therefore, our results are consistent with the notion that oxyHc is easily produced through a nearly simultaneous two-step ET mechanism.[15,16] The QM(UBH&HLYP)/MM reaction energy of −18.9 kcal mol^{-1} overestimates the observed binding enthalpy of −11.5 to −6.0 kcal mol^{-1} for Hc[79] and of −14 kcal mol^{-1} for a synthetic model complex (N4 ligand).[12]

3.3. Effect of the Protein Environment on the Computed Energies. As discussed above, the overall O_2 binding/release reaction at the active site of Hc is well described at the QM(DFT)/MM level when the UBH&HLYP functional is used. To assess the influence of the MM environment on the energies of the stationary points optimized at the QM(UBH&HLYP)/MM level, we divide the QM-(UBH&HLYP)/MM energies into the $E^{QM(pc)}$ and E^{MM} contributions. $E^{QM(pc)}$ is the QM energy computed in the presence of the MM point charges, and E^{MM} is the remaining total MM energy (including the nonelectrostatic QM/MM interaction terms). In addition, we performed single-point QM(UBH&HLYP) calculations of the QM region at the QM/MM optimized geometries, both in the gas phase without any MM point charges (called QM(gas)) and in a solvent environment represented by the polarizable continuum model (PCM) using the cavity generated by UFF atomic radii (called QM(PCM)),[83] with the dielectric constant (ε) set to 4.[84] The computed energies relative to ^{3}**1** are listed in Table 3.

The $E^{QM(gas)}$, $E^{QM(pc)}$, and $E^{QM(PCM)}$ values are generally very similar to each other (typically within 1 kcal mol^{-1}), indicating that the electrostatic interactions between the QM region and the protein environment have only a minor influence on the energy profile of the overall reaction. On the other hand, the MM energy terms (i.e., the difference between the QM/MM and QM(pc) entries in Table 3) significantly lower the relative energy of all computed stationary points, by 1.2−6.2 kcal mol^{-1}, with the stabilization increasing along the reaction pathway. Curiously, inclusion of the MM energy terms deteriorates the agreement with the available experimental thermodynamic data. The activation barriers for the rate-limiting transition state ^{3}**TS1** from the QM(gas), QM(pc), and QM(PCM) calculations agree well with the observed activation enthalpy of 7.2 kcal mol^{-1}, which is underestimated at the full QM/MM level by 3.7 kcal mol^{-1} (Table 3). Similarly, the computed reaction energies without the E^{MM} term show better agreement with the observed reaction enthalpy. However, the deviations between the QM/MM results and the experimental data are not alarmingly large, especially considering the strong sensitivity of the QM/MM results to the choice of DFT functional (section 3.2). Therefore, we have refrained from attempts to decrease the influence of the MM energy terms by increasing the size of the QM region.

We emphasize in this context that the experimental activation enthalpy for oxygen binding was determined[15] in the high oxygen affinity R-state of *Carcinus aestuarii* deoxyHc, for which an X-ray crystal structure is unfortunately not yet available. Our QM/MM calculations are based on the crystal structure[5] of the low oxygen affinity T-state of oxyHc from *Limulus polyphemus*. Hence there will be some inevitable differences in the protein environment in these two systems. In addition, our QM/MM model does not capture the full complexity of the experimental setup (e.g., with regard to buffer, counterions, pH value, and interunit interactions), and we compare the measured enthalpies[15] to our computed relative energies. All these factors impede direct quantitative comparisons between experiment and theory. In our approach, we basically assume that the energy changes during oxygen binding are mainly governed by the changes of local interactions in the active site (which is the same in both systems) and that qualitative comparisons will therefore still be meaningful.

4. CONCLUSION

In this paper, we have studied the mechanism of reversible dioxygen binding in Hc by means of QM(DFT)/MM calculations. We have considered the possible electron transfer processes and have located the minimum-energy crossing point

dx.doi.org/10.1021/jp5003885 | J. Phys. Chem. B 2014, 118, 5034−5043

between the triplet and singlet states to characterize the spin-forbidden reaction. The QM(DFT)/MM geometry optimizations were carried out using a modified version of the Gaussian09 interface in the ChemShell program package. The new procedure for evaluating the forces at the MM atoms is much more efficient than the method previously implemented in ChemShell.

The experimental X-ray structure of deoxyHc is well reproduced by QM(DFT)/MM geometry optimizations with functionals that do not account for dispersion, whereas the dispersion-corrected B3LYP-D3 and the M06-2X functionals tend to make the $Cu_A\cdots Cu_B$ distance too short by ca. 0.3 Å; in contrast, unconstrained QM-only geometry optimizations of the QM region lead to dissociation of deoxyHc. The QM(DFT)/MM energy profiles for the O_2 binding process in deoxyHc dramatically depend on the chosen functional. The pure UBLYP functional is unsuitable because it predicts the triplet product to be more stable than the experimentally observed singlet oxyHc product. Hybrid functionals correctly give singlet oxyHc as the most stable species. However, the UB3LYP, UCAM-B3LYP, and UM06-2X functionals predict a barrierless downhill pathway from deoxyHc to oxyHc, in contrast to the experimentally observed small barrier for O_2 binding; in addition, UM06-2X overestimates the stability of oxyHc. It is thus only the UBH&HLYP functional that gives a realistic QM(DFT)/MM energy profile, which is qualitatively consistent with the experimental findings.

According to the QM(UBH&HLYP)/MM calculations, the reaction proceeds stepwise with two sequential ET processes in the triplet state followed by an intersystem crossing to the singlet oxyHc product. The first ET step leads to a nonbridged superoxo $Cu_B^{II}-O_2^{\bullet-}$ intermediate via a low-barrier rate-limiting transition state. The second ET step is even more facile and yields a triplet oxyHc species that already contains the characteristic Cu_2O_2 butterfly core. The final ISC step is expected to be fast because it is exothermic and retains the atom connectivity. Overall, the computed QM/MM energy profile (Figure 3) suggests a very rapid reaction because the barriers are very small for each ET step. Our results are thus consistent with the mechanistic notion of two almost simultaneous electron transfers that has been suggested in previous experimental studies.[15,16]

■ ASSOCIATED CONTENT

Supporting Information

System setup by using CHARMM; comparison between Gaussian09 and TURBOMOLE results; optimized Cartesian coordinates; magnetic orbitals for nonbridged superoxo intermediate; total energies for singlet and triplet states at the MECP; full citations for refs 14, 59, 61, and 82. This material is available free of charge via the Internet at http://pubs.acs.org.

■ AUTHOR INFORMATION

Corresponding Author

*W. Thiel: e-mail, thiel@kofo.mpg.de; phone, +49(0)208/306-2150.

Notes

The authors declare no competing financial interest.

■ ACKNOWLEDGMENTS

This work was supported by the Japan Society for the Promotion of Science (JSPS) through a Postdoctoral Fellowship for Research Abroad. T. S. is grateful to Dr. Kakali Sen and Iakov Polyak for fruitful discussions about the QM/MM setup and to Prof. Jeremy Harvey for providing his code for MECP optimization.

■ REFERENCES

(1) Magnus, K. A.; Ton-That, H.; Carpenter, J. E. Recent Structural Work on the Oxygen Transport Protein Hemocyanin. *Chem. Rev.* **1994**, *94*, 727−735.

(2) Solomon, E. I.; Sundaram, U. M.; Machonkin, T. E. Multicopper Oxidases and Oxygenases. *Chem. Rev.* **1996**, *96*, 2563−2606.

(3) Decker, H.; Schweikardt, T.; Nillius, D.; Salzbrunn, U.; Jaenicke, E.; Tuczek, F. Similar Enzyme Activation and Catalysis in Hemocyanin and Tyrosinase. *Gene* **2007**, *398*, 183−191.

(4) Solomon, E. I.; Ginsbach, J. W.; Heppner, D. E.; Kieber-Emmons, M. T.; Kjaergarrd, C. H.; Smeets, P. J.; Tian, L.; Woertink, J. S. Copper Dioxygen (Bio)inorganic Chemistry. *Faraday Discuss.* **2011**, *148*, 11−39.

(5) Magnus, K. A.; Hazes, B.; Ton-That, H.; Bonaventura, C.; Bonaventura, J.; Hol, W. G. J. Crystallographic Analysis of Oxygenated and Deoxygenated States of Arthropod Hemocyanin Shows Unusual Difference. *Proteins: Struct., Funct., Genet.* **1994**, *19*, 302−309.

(6) Hazes, B.; Magnus, K. A.; Bonaventura, C.; Bonaventura, J.; Dauter, Z.; Kalk, K. H.; Hol, W. G. J. Crystal Structure of Deoxygenated Limulus Polyphemus Subunit II Hemocyanin at 2.18 Å Resolution: Clues for a Mechanism for Allosteric Regulation. *Protein Sci.* **1993**, *2*, 597−619.

(7) Cuff, M. E.; Miller, K. I.; van Holde, K. E.; Hendrickson, W. A. Crystal Structure of a Functional Unit from Octopus Hemocyanin. *J. Mol. Biol.* **1998**, *278*, 855−870.

(8) Monod, J.; Wyman, J.; Changeux, J.-P. On the Nature of Allosteric Transitions: A Plausible Model. *J. Mol. Biol.* **1965**, *12*, 88−118.

(9) Karlin, K. D.; Kaderli, S.; Zuberbühler, A. D. Kinetics and Thermodynamics of Copper(I)/Dioxygen Interaction. *Acc. Chem. Res.* **1997**, *30*, 139−147.

(10) Kitajima, N.; Fujisawa, K.; Fujimoto, C.; Moro-oka, Y.; Hashimoto, S.; Kitagawa, T.; Tatsumi, K.; Nakamura, A. A New Model for Dioxygen Binding in Hemocyanin. Synthesis, Characterization, and Molecular Structure of the μ:η^2-η^2 Peroxo Dinuclear Copper(II) Complexes, $[Cu(HB(3,5\text{-}R2pz)_3)]_2(O_2)$ (R = isopropyl and Ph). *J. Am. Chem. Soc.* **1992**, *114*, 1277−1291.

(11) Fujisawa, K.; Tanaka, M.; Moro-oka, Y.; Kitajima, N. A Monomeric Side-On Superoxocopper(II) Complex: $Cu(O_2)$(HB(3-^{t}Bu-5-^{i}Prpz). *J. Am. Chem. Soc.* **1994**, *116*, 12079−12080.

(12) Karlin, K. D.; Tolman, W. B.; Kaderli, S.; Zuberbühler, A. D. Kinetic and Thermodynamic Parameters of Copper-Dioxygen Interaction with Different Oxygen Binding Modes. *J. Mol. Catal. A: Chem.* **1997**, *117*, 215−222.

(13) Kodera, M.; Katayama, K.; Tachi, Y.; Kano, K.; Hirota, S.; Fujinami, S.; Suzuki, M. Crystal Structure and Reversible O2-Binding of a Room Temperature Stable μ:η^2-η^2-Peroxodicopper(II) Complex of a Sterically Hindered Hexapyridine Dinucleating Ligand. *J. Am. Chem. Soc.* **1999**, *121*, 11006−11007.

(14) Funahashi, Y.; Nishikawa, T.; Wasada-Tsutsui, Y.; Kajita, Y.; Yamaguchi, S.; Arii, H.; Ozawa, T.; Jitsukawa, K.; Tosha, T.; Hirota, S.; et al. H. Formation of a Bridged Butterfly-Type μ:η^2-η^2-Peroxo Dicopper Core Structure with a Carboxylate Group. *J. Am. Chem. Soc.* **2008**, *130*, 16444−16445.

(15) Hirota, S.; Kawahara, T.; Beltramini, M.; Di Muro, P.; Magliozzo, R. S.; Peisach, J.; Powers, L. S.; Tanaka, N.; Nagao, S.; Bubacco, L. Molecular Basis of the Bohr Effect in Arthropod Hemocyanin. *J. Biol. Chem.* **2008**, *283*, 31941−31948.

(16) Lucas, H. R.; Meyer, G. J.; Karlin, K. D. CO and O_2 Binding to Pseudo-tetradentate Ligand−Copper(I) Complexes with a Variable N-Donor Moiety: Kinetic/Thermodynamic Investigation Reveals Ligand-Induced Changes in Reaction Mechanism. *J. Am. Chem. Soc.* **2010**, *132*, 12927−12940.

(17) Solomon, E. I.; Dooley, D. M.; Wang, R. H.; Gray, H. B.; Cerdonio, M.; Mogno, F.; Romani, G. L. Susceptibility Studies of Laccase and Oxyhemocyanin Using an Ultrasensitive Magnetometer. Antiferromagnetic Behavior of the Type 3 Copper in Rhus Laccase. *J. Am. Chem. Soc.* **1976**, *98*, 1029−1031.
(18) Matoba, Y.; Kumagai, T.; Yamamoto, A.; Yoshitsu, H.; Sugiyama, M. Crystallographic Evidence That the Dinuclear Copper Center of Tyrosinase Is Flexible during Catalysis. *J. Biol. Chem.* **2006**, *281*, 8981−8990.
(19) Que, L., Jr.; Tolman, W. B. Biologically Inspired Oxidation Catalysis. *Nature* **2008**, *455*, 333−340.
(20) Itoh, S.; Fukuzumi, S. Monooxygenase Activity of Type 3 Copper Proteins. *Acc. Chem. Res.* **2007**, *40*, 592−600.
(21) Cramer, C. J.; Wloch, M.; Piecuch, P.; Puzzarini, C.; Gagliardi, L. Theoretical Models on the Cu_2O_2 Torture Track: Mechanistic Implications for Oxytyrosinase and Small-Molecule Analogues. *J. Phys. Chem. A* **2006**, *110*, 1991−2004.
(22) Cramer, C. J.; Kinal, A.; Wloch, M.; Piecuch, P.; Gagliardi, L. Theoretical Characterization of End-On and Side-On Peroxide Coordination in Ligated Cu_2O_2 Models. *J. Phys. Chem. A* **2006**, *110*, 11557−11568.
(23) Gherman, B. F.; Cramer, C. J. Quantum Chemical Studies of Molecules Incorporating a $Cu_2O_2^{2+}$ Core. *Coord. Chem. Rev.* **2009**, *253*, 723−753.
(24) Siegbahn, P. E. M. The Performance of Hybrid DFT for Mechanisms Involving Transition Metal Complexes in Enzymes. *J. Biol. Inorg. Chem.* **2006**, *11*, 695−701.
(25) Kong, L.; Nooijen, M. Study of Energetics of End-on and Side-on Peroxide Coordination in Ligated Cu_2O_2 Models with State-Specific Equation of Motion Coupled Cluster Method. *Int. J. Quantum Chem.* **2008**, *108*, 2097−2107.
(26) Yanai, T.; Kurashige, Y.; Neuscamman, E.; Chan, G. K. L. Multireference Quantum Chemistry Through a Joint Density Matrix Renormalization Group and Canonical Transformation Theory. *J. Chem. Phys.* **2010**, *132*, 024105.
(27) Liakos, D. G.; Neese, F. Interplay of Correlation and Relativistic Effects in Correlated Calculations on Transition-Metal Complexes: The $(Cu_2O_2)^{2+}$ Core Revisited. *J. Chem. Theory Comput.* **2011**, *7*, 1511−1523.
(28) Rohrmüller, M.; Herres-Pawlis, S.; Witte, M.; Schmidt, W. G. Bis-μ-oxo and $\mu{:}\eta^2{-}\eta^2$-Peroxo Dicopper Complexes Studied within (Time-Dependent) Density-Functional and Many-Body Perturbation Theory. *J. Comput. Chem.* **2013**, *34*, 1035−1045.
(29) Bernardi, F.; Bottoni, A.; Casadio, R.; Fariselli, P.; Rigo, A. Ab Initio Study of the Mechanism of the Binding of Triplet O_2 to Hemocyanin. *Inorg. Chem.* **1996**, *35*, 5207−5212.
(30) Metz, M.; Solomon, E. I. Dioxygen Binding to Deoxyhemocyanin: Electronic Structure and Mechanism oft he Spin-Forbidden Two-Electron Reduction of O_2. *J. Am. Chem. Soc.* **2001**, *123*, 4938−4950.
(31) Solomon, E. I.; Chen, P.; Metz, M.; Lee, S.-K.; Palmer, A. E. Oxygen Binding, Activation, and Reduction to Water by Copper Proteins. *Angew. Chem., Int. Ed.* **2001**, *40*, 4570−4590.
(32) Takano, Y.; Kubo, S.; Onishi, T.; Isobe, H.; Yoshioka, Y.; Yamaguchi, K. Theoretical Studies on the Magnetic Interaction and Reversible Dioxygen Binding of the Active Site in Hemocyanin. *Chem. Phys. Lett.* **2001**, *335*, 395−403.
(33) Saito, T.; Kataoka, Y.; Nakanishi, Y.; Matsui, T.; Kitagawa, Y.; Kawakami, T.; Yamaguchi, K. Which Hybrid GGA DFT is Suitable for Cu_2O_2 Systems If the Spin Contamination Error is Removed? *Chem. Phys.* **2010**, *368*, 1−6.
(34) Takano, Y.; Koizumi, K.; Nakamura, H. Theoretical Studies on the Magnetic Coupling and the Chemical Indices of the Biomimetic Models of Oxyhemocyanin and Oxytyrosinase. *Inorg. Chim. Acta* **2009**, *362*, 4578−4584.
(35) Yoon, J.; Fujii, S.; Solomon, E. I. Geometric and Electronic Structure Differences between the Type 3 Copper Sites of the Multicopper Oxidases and Hemocyanin/Tyrosinase. *Proc. Natl. Acad. Sci. U. S. A.* **2009**, *106*, 6585−6590.
(36) Warshel, A.; Levitt, M. Theoretical Studies of Enzymic Reactions: Dielectric, Electrostatic and Steric Stabilization of the Carbonium Ion in the Reaction of Lysozyme. *J. Mol. Biol.* **1976**, *103*, 227−249.
(37) Lin, H.; Truhlar, D. G. QM/MM: What Have We Learned, Where Are We, and Where Do We Go from Here? *Theor. Chem. Acc.* **2007**, *117*, 185−199.
(38) Senn, H. M.; Thiel, W. QM/MM Methods for Biomolecular Systems. *Angew. Chem., Int. Ed.* **2009**, *48*, 1198−1229.
(39) Lonsdale, R.; Harvey, J. N.; Mulholland, A. J. A Practical Guide to Modelling Enzyme-Catalysed Reactions. *Chem. Soc. Rev.* **2012**, *41*, 3025−3038.
(40) Sali, A.; Blundell, T. L. Comparative Protein Modelling by Satisfaction of Spatial Restraints. *J. Mol. Biol.* **1993**, *234*, 779−815.
(41) Olsson, M. H. M.; Søndergaard, C. R.; Rostkowski, M.; Jensen, J. H. PROPKA3: Consistent Treatment of Internal and Surface Residues in Empirical pKa Predictions. *J. Chem. Theory Comput.* **2011**, *7*, 525−537.
(42) Cox, S. R.; Williams, D. E. Representation of the Molecular Electrostatic Potential by a Net Atomic Charge Model. *J. Comput. Chem.* **1981**, *2*, 304−323.
(43) Sigfridsson, E.; Ryde, U. Comparison of Methods for Deriving Atomic Charges from the Electrostatic Potential and Moments. *J. Comput. Chem.* **1998**, *19*, 377−395.
(44) Ungar, L. W.; Scherer, N. F.; Voth, G. A. Classical Molecular Dynamics Simulation of the Photoinduced Electron Transfer Dynamics of Plastocyanin. *Biophys. J.* **1997**, *72*, 5−17.
(45) Brooks, B. R.; Bruccoleri, R. E.; Olafson, B. D.; States, D. J.; Swaminathan, S.; Karplus, M. CHARMM: A Program for Macromolecular Energy, Minimization, and Dynamics Calculations. *J. Comput. Chem.* **1983**, *4*, 187−217.
(46) Metz, S.; Wang, D.; Thiel, W. Reductive Half-Reaction of Aldehyde Oxidoreductase toward Acetaldehyde: A Combined QM/MM Study. *J. Am. Chem. Soc.* **2009**, *131*, 4628−4640.
(47) Polyak, I.; Reetz, M. T.; Thiel, W. Quantum Mechanical/Molecular Mechanical Study on the Mechanism of the Enzymatic Baeyer−Villiger Reaction. *J. Am. Chem. Soc.* **2012**, *134*, 2732−2741.
(48) Liao, R.-Z.; Thiel, W. Why Is the Oxidation State of Iron Crucial for the Activity of Heme-Dependent Aldoxime Dehydratase? A QM/MM Study. *J. Phys. Chem. B* **2012**, *116*, 9396−9408.
(49) Brooks, B. R.; Karplus, M. Deformable Stochastic Boundaries in Molecular Dynamics. *J. Chem. Phys.* **1983**, *79*, 6312−6325.
(50) Becke, A. Density-Functional Exchange-Energy Approximation with Correct Asymptotic Behavior. *Phys. Rev. A* **1988**, *38*, 3098−3100.
(51) Lee, C.; Yang, W.; Parr, R. G. Development of the Colle-Salvetti Correlation-Energy Formula into a Functional of the Electron Density. *Phys. Rev. B* **1988**, *37*, 785−789.
(52) Becke, A. Density-Functional Thermochemistry. III. The Role of Exact Exchange. *J. Chem. Phys.* **1993**, *93*, 5648−5652.
(53) Becke, A. A New Mixing of Hartree-Fock and Local Density-Functional Theories. *J. Chem. Phys.* **1993**, *98*, 1372−1377.
(54) Zhao, Y.; Truhlar, D. G. The M06 Suite of Density Functionals for Main Group Thermochemistry, Thermochemical Kinetics, Noncovalent Interactions, Excited States, and Transition Elements: Two New Functionals and Systematic Testing of Four M06-Class Functionals and 12 Other Functionals. *Theor. Chem. Acc.* **2008**, *120*, 215−241.
(55) Yanai, T.; Tew, D. P.; Handy, N. C. A New Hybrid Exchange−Correlation Functional Using the Coulomb-Attenuating Method (CAM-B3LYP). *Chem. Phys. Lett.* **2004**, *393*, 51−57.
(56) Schäfer, A.; Horn, H.; Ahlrichs, R. Fully Optimized Contracted Gaussian Basis Sets for Atoms Li to Kr. *J. Chem. Phys.* **1992**, *97*, 2571−2577.
(57) Yamaguchi, K.; Takahara, Y.; Fueno, T. In *Applied Quantum Chemistry*, Smith, V. H., Schaefer, H. F., III, Morokuma, K., Eds.; D. Reidel: Boston, MA, 1986; p 15.
(58) Yamaguchi, K.; Jensen, F.; Dorigo, A.; Houk, K. N. A Spin Correction Procedure for Unrestricted Hartree-Fock and Møller-

Plesset Wavefunctions for Singlet Diradicals and Polyradicals. *Chem. Phys. Lett.* **1988**, *149*, 537−542.
(59) Sherwood, P.; de Vries, A. H.; Guest, M. F.; Schreckenbach, G.; Catlow, C. R. C.; French, S. A.; Sokol, A. A.; Bromley, S. T.; Thiel, W.; Turner, A. J.; et al. QUASI: A General Purpose Implementation of the QM/MM Approach and its Application to Problems in Catalysis. *J. Mol. Struct. (THEOCHEM)* **2003**, *632*, 1−28.
(60) *Chemshell, a Computational Chemistry Shell*; Science & Technology Facilities Council: Swindon, U.K., www.chemshell.org (accessed on January 12, 2014).
(61) Frisch, M. J.; Trucks, G. W.; Schlegel, H. B.; Scuseria, G. E.; Robb, M. A.; Cheeseman, J. R.; Scalmani, G.; Barone, V.; Mennucci, B.; Petersson, G. A.; et al. *Gaussian 09*, Revision B.01; Gaussian, Inc.: Wallingford, CT, 2009.
(62) Smith, W.; Forester, T. R. DL_POLY_2.0: A General-Purpose Parallel Molecular Dynamics Simulation Package. *J. Mol. Graphics* **1996**, *14*, 136−141.
(63) Okamoto, T.; Yamada, K.; Koyano, Y.; Asada, T.; Koga, N.; Nagaoka, M. A Minimal Implementation of the AMBER−GAUSSIAN Interface for Ab Initio QM/MM-MD Simulation. *J. Comput. Chem.* **2011**, *32*, 932−942.
(64) Billeter, S. R.; Turner, A. J.; Thiel, W. Linear Scaling Geometry Optimisation and Transition State Search in Hybrid Delocalised Internal Coordinates. *Phys. Chem. Chem. Phys.* **2000**, *2*, 2177−2186.
(65) Kästner, J.; Carr, J. M.; Keal, T. W.; Thiel, W.; Wander, A.; Sherwood, P. DL-FIND: An Open-Source Geometry Optimizer for Atomistic Simulations. *J. Phys. Chem. A* **2009**, *113*, 11856−11865.
(66) Nocedal, J. Updating Quasi-Newton Matrices with Limited Storage. *Math. Comput.* **1980**, *35*, 773−782.
(67) Henkelman, G.; Jónsson, H. Improved Tangent Estimate in the Nudged Elastic Band Method for Finding Minimum Energy Paths and Saddle Points. *J. Chem. Phys.* **1999**, *111*, 7010−7022.
(68) Kästner, J.; Sherwood, P. Superlinearly Converging Dimer Method for Transition State Search. *J. Chem. Phys.* **2008**, *128*, 014106.
(69) Harvey, J. N.; Aschi, M.; Schwarz, H.; Koch, W. The Singlet and Triplet States of Phenyl Cation. A Hybrid Approach for Locating Minimum Energy Crossing Points between Non-Interacting Potential Energy Surfaces. *Theor. Chem. Acc.* **1998**, *99*, 95−99.
(70) Harvey, J. N.; Poli, R.; Smith, K. M. Understanding the Reactivity of Transition Metal Complexes Involving Multiple Spin States. *Coord. Chem. Rev.* **2003**, *238*−*239*, 347−361.
(71) Harvey, J. N. Spin-Forbidden Reactions: Computational Insight into Mechanisms and Kinetics. *WIREs Comput. Mol. Sci.* **2014**, *4*, 1−14.
(72) Ahlrichs, R.; Bär, M.; Häser, M.; Horn, H.; Kölmel, C. Electronic Structure Calculations on Workstation Computers: The Program System Turbomole. *Chem. Phys. Lett.* **1989**, *162*, 165−169.
(73) Grimme, S.; Antony, J.; Ehrlich, S.; Krieg, H. A Consistent and Accurate Ab Initio Parametrization of Density Functional Dispersion Correction (DFT-D) for the 94 Elements H-Pu. *J. Chem. Phys.* **2010**, *132*, 154104.
(74) Ryde, U. Accurate Metal-Site Structures in Proteins Obtained by Combining Experimental Data and Quantum Chemistry. *Dalton Trans.* **2007**, *No. 6*, 607.
(75) Krupenie, P. H. The Spectrum of Molecular Oxygen. *J. Phys. Chem. Ref. Data* **1972**, *1*, 423−534.
(76) Saito, T.; Nishihara, S.; Yamanaka, S.; Kitagawa, Y.; Kawakami, T.; Yamada, S.; Isobe, H.; Okumura, M.; Yamaguchi, K. Singlet-Triplet Energy Gap for Trimethylenemethane, Oxyallyl Diradical, and Related Species: Single- and Multireference Computational Results. *Theor. Chem. Acc.* **2011**, *130*, 739−748.
(77) Saito, T.; Nishihara, S.; Kataoka, Y.; Nakanishi, Y.; Kitagawa, Y.; Kawakami, T.; Yamanaka, S.; Okumura, M.; Yamaguchi, K. Reinvestigation of the Reaction of Ethylene and Singlet Oxygen by the Approximate Spin Projection Method. Comparison with Multireference Coupled-Cluster Calculations. *J. Phys. Chem. A* **2010**, *114*, 7967−7974.
(78) Chen, H.; Ikeda-Saito, M.; Shaik, S. Nature of the Fe-O_2 Bonding in Oxy-Myoglobin: Effect of the Protein. *J. Am. Chem. Soc.* **2008**, *130*, 14778−14790.
(79) Klarman, A.; Daniel, E. Oxygen Binding Properties of Stripped (Calcium Ion and Magnesium Ion Free) Hemocyanin from the Scorpion Leirus Quinquestriatus. *Biochemistry* **1980**, *19*, 5176−5180.
(80) Würtele, C.; Gaoutchenova, E.; Harms, K.; Holthausen, M. C.; Sundermeyer, J.; Schindler, S. Crystallographic Characterization of a Synthetic 1:1 End-On Copper Dioxygen Adduct Complex. *Angew. Chem., Int. Ed.* **2006**, *45*, 3867−3869.
(81) Chen, P.; Root, D. E.; Campochiaro, C.; Fujisawa, K.; Solomon, E. I. Spectroscopic and Electronic Structure Studies of the Diamagnetic Side-On CuII-Superoxo Complex $Cu(O_2)[HB(3\text{-}R\text{-}5\text{-}^{i}Prpz)_3]$: Antiferromagnetic Coupling versus Covalent Delocalization. *J. Am. Chem. Soc.* **2003**, *125*, 466−474.
(82) Woertink, J. S.; Tian, L.; Maiti, D.; Lucas, H. R.; Himes, R. A.; Karlin, K. D.; Neese, F.; Würtele, C.; Holthausen, M. C.; Bill, E.; et al. Spectroscopic and Computational Studies of an End-on Bound Superoxo-Cu(II) Complex: Geometric and Electronic Factors That Determine the Ground State. *Inorg. Chem.* **2010**, *49*, 9450−9459.
(83) Scalmani, G.; Frisch, M. J. Continuous Surface Charge Polarizable Continuum Models of Solvation. I. General Formalism. *J. Chem. Phys.* **2010**, *132*, 11410.
(84) Siegbahn, P. E. M.; Blomberg, M. R. A. Transition-Metal Systems in Biochemistry Studied by High-Accuracy Quantum Chemical Methods. *Chem. Rev.* **2000**, *100*, 421−438.